THE JOURNAL OF PHYSICAL CHEMISTRY C

Article

Cite This: J. Phys. Chem. C 2019, 123, 16107−16117

pubs.acs.org/JPCC

C_2H_2 Selective Hydrogenation over the M@Pd and M@Cu (M = Au, Ag, Cu, and Pd) Core−Shell Nanocluster Catalysts: The Effects of Composition and Nanocluster Size on Catalytic Activity and Selectivity

Riguang Zhang,[†,‡] Mifeng Xue,[†] Baojun Wang,*[,†] Lixia Ling,[†] and Maohong Fan*[,‡,§,∥]

[†]Key Laboratory of Coal Science and Technology of Ministry of Education and Shanxi Province, Taiyuan University of Technology, Taiyuan 030024, Shanxi, P. R. China

[‡]Department of Chemical Engineering and Department of Petroleum Engineering and [§]School of Energy Resources, University of Wyoming, Laramie, Wyoming 82071, United States

[∥]School of Civil and Environmental Engineering, Georgia Institute of Technology, Atlanta, Georgia 30332, United States

Supporting Information

ABSTRACT: To clarify the effects of the composition and nanocluster size of the core−shell catalysts on C_2H_4 selectivity and activity in C_2H_2 selective hydrogenation, the kinetic mechanisms of C_2H_2 selective hydrogenation over different compositions of M@Pd (M = Au, Ag, and Cu) and M@Cu (M = Au, Ag, and Pd) nanoclusters with different sizes are investigated using density functional theory calculations. The results suggest that the composition and nanocluster size of the core−shell catalyst affect C_2H_4 selectivity and activity, and Cu as the core for M@Pd catalysts exhibits excellent C_2H_4 selectivity and activity than that of Au and Ag; moreover, M@Pd catalysts show better C_2H_4 selectivity and activity than M@Cu. Namely, the core−shell nanocluster catalyst with Cu as the core and Pd as the shell is beneficial to improve C_2H_4 selectivity and activity in C_2H_2 selective hydrogenation. On the other hand, C_2H_4 selectivity and activity increase over M@Pd catalysts with the increase in the nanocluster size, which means that it is necessary to have the catalyst with a larger cluster size in the preparation of Cu@Pd core−shell catalysts. The electronic structure analysis revealed the microscopic reasons about the effects of core−shell catalyst compositions and nanocluster size on the catalytic performance of C_2H_2 selective hydrogenation. This study can provide theoretical guidance for the design of core−shell nanocluster catalysts to improve C_2H_4 selectivity and activity in C_2H_2 selective hydrogenation by adjusting the composition and nanocluster size in an efficient way.

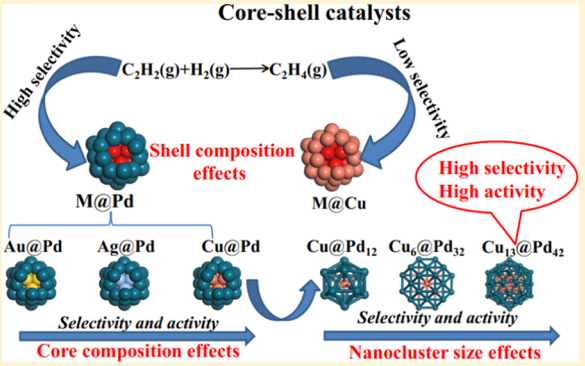

1. INTRODUCTION

C_2H_2 selective hydrogenation is an important chemical process for removing a trace amount of C_2H_2 impurities from C_2H_4 feedstock.[1−4] During this process, the noble metal Pd catalyst is considered to be one of the most promising due to its good activity of C_2H_4 formation.[1,3,5] Nevertheless, it has several disadvantages including high price and poor C_2H_4 selectivity due to the overhydrogenation of C_2H_4, lowering the selectivity of C_2H_4.[5−7] As a result, several transition metals Au,[8−10] Ag,[3,5,11,12] and Cu[7,13,14] were added into the Pd catalyst to form a Pd-based catalyst as a selectivity modifier to improve C_2H_4 selectivity. Zhang et al.[15] indicated that the addition of Ag into the Pd catalyst can improve C_2H_4 selectivity and lower the catalytic activity in comparison with the single Pd catalyst. Zhang et al.[16] synthesized a series of Ag− and Au−Pd/SiO_2 bimetallic catalysts for C_2H_2 selective hydrogenation; both promoter Ag and Au at high coverage effectively improve C_2H_4 selectivity, whereas the low coverage of Au and Ag cannot improve C_2H_4 selectivity due to the larger Pd ensembles. Sárkány et al.[10] suggested that the promoter Au-decorated Pd catalyst inhibits the carbonaceous deposition and improves C_2H_4 selectivity. Kim et al.[7] experimentally found that Cu-promoted Pd/Al_2O_3 catalysts exhibit higher selectivity and activity toward C_2H_4 formation than the Ag-promoted Pd/Al_2O_3 catalyst. Pei et al.[17] indicated that the Cu-alloyed Pd catalyst can effectively enhance C_2H_4 selectivity (∼85%) due to the isolation of Pd by promoter Cu and the electron transfer from the Cu to Pd atom, which are in favor of H_2 dissociation and the desorption of C_2H_4. On the other hand, at a higher reaction temperature (above 440 K), the metal Cu become the main active component of C_2H_2 selective hydrogenation and exhibits higher C_2H_4 selectivity.[18−21] For instance, McCue et

Received: February 23, 2019
Revised: June 3, 2019
Published: June 10, 2019

DOI: 10.1021/acs.jpcc.9b01757
J. Phys. Chem. C 2019, 123, 16107−16117

al.[20] prepared a large number of Pd-modified Cu bimetallic catalysts, and when the Cu/Pd ratio was 50:1, the catalyst showed excellent C_2H_4 selectivity and activity. Kyriakou et al.[22] demonstrated that the modification of a single Pd atom for the Cu(111) surface improves C_2H_4 selectivity for C_2H_2 selective hydrogenation compared with the single Cu and Pd surface. Moreover, Fu et al.[23] revealed that the ensembles composed of surface and its joint subsurface Pd atoms are beneficial to improve the catalytic activity of H_2 dissociation; this ensemble is also beneficial to improve the C_2H_4 selectivity and catalytic activity for acetylene selective hydrogenation. The above results show that both Pd-based and Cu-based catalysts have been widely applied to C_2H_2 selective hydrogenation, which have presented better catalytic performance.

Recently, the core−shell catalysts have attracted extensive attention and become one of the most potential catalysts due to their unique structures.[24−27] The composition of core−shell catalysts affects their catalytic performance.[28−31] For the M@Pd core−shell catalysts, Li et al.[28] confirmed that the Cu@Pd catalyst shows higher activity toward formic acid oxidation four times than the pure Pd catalyst. Kuhn et al.[29] suggested that the Pd−Ag/Al_2O_3 core−shell catalysts effectively prevent the formation of coke and green oil during the C_2H_2 selective hydrogenation and exhibit higher long-time stability relative to the pure Pd catalyst. Sárkány et al.[9] synthesized a series of Au@Pd catalysts with different Pd shell thicknesses, indicating that the core−shell catalyst with the Pd layer can significantly enhance the catalytic activity of acetylene selective hydrogenation than the pure Pd catalyst. McCue et al.[32] have synthesized the Au@Pd nanoparticles (NPs) by the addition of Pd to the Au with different rates of Pd addition, suggesting that the faster addition favored the formation of monometallic Pd nanoparticles outside the core−shell nanoparticles, and the catalyst shows poor C_2H_4 selectivity for C_2H_2 selective hydrogenation; yet, the slow addition of shell Pd results in the formation of a core−shell structure, and the catalyst exhibits higher C_2H_4 selectivity. Yet, up to now, there are still a few theoretical studies of C_2H_2 selective hydrogenation over different compositions of M@Pd core−shell catalysts. On the other hand, for the M@Cu core−shell catalysts, density functional theory (DFT) studies by Guo et al.[30] have shown that the M@Cu12 (M = Co, Rh, Ir) core−shell catalysts have higher activity toward water−gas shift reaction (WGSR) than the N@Cu12 (N = Ni, Pd, Pt, Cu, Ag, Au) core−shell catalysts does. Moreover, Lin et al.[31] showed that the Cu@Ni core−shell catalyst exhibits good CO conversion than the Ni@Cu core−shell catalyst in WGSR. However, the reported experimental and theoretical studies of C_2H_2 selective hydrogenation over M@Cu core−shell catalysts are still limited. Moreover, as mentioned above, the role of M@Pd and M@Cu core−shell catalyst and the composition effects of M@Pd and M@Cu catalysts on the C_2H_2 selective hydrogenation have rarely been mentioned.

Furthermore, the nanocluster particle size of core−shell catalysts significantly affects the stability and catalytic performance.[33−35] For instance, An et al.[35] suggested that the catalytic activity of the Pd@Pt core−shell catalyst toward oxygen reduction reaction (ORR) strongly depends on the catalyst particle size. Gan et al.[36] showed that the activity of ORR and the corresponding stability have the close relationship with $PtNi_3$-NPs catalyst particle size, which presents a Volcano curve, and the catalyst exhibits the best activity when the nanocluster particle size of $PtNi_3$-NPs was 6−8 nm. Moreover, Chen et al.[37] suggested that for the ethanol oxidation reaction the Au@Pd catalyst presents higher catalytic activity five times than the pure Pd catalysts; moreover, with the increase in nanocluster particle size (2.9, 5.8, and 6.5 nm), the catalytic activity increased. However, up to now, the nanocluster particle size effect for M@Pd and M@Cu core−shell catalysts on C_2H_4 selectivity and activity in C_2H_2 selective hydrogenation is still unclear.

In this paper, aiming at discussing above issues, different compositions of M@Pd (M = Au, Ag, and Cu) and M@Cu (M = Au, Ag, and Pd) core−shell nanoclusters with different sizes are selected to represent different compositions and nanocluster sizes of M@Pd and M@Cu core−shell catalysts. The kinetic mechanism of C_2H_2 selective hydrogenation over M@Pd and M@Cu catalysts is investigated; here, the density functional theory calculations are carried out. The nanocluster size and composition effects of the core−shell catalyst on the activity and selectivity of C_2H_2 selective hydrogenation are identified. Electronic structure analysis is carried out to reveal the microscopic reasons. We hope our results to give a theoretical clue to realize the design of high-performance core−shell catalysts in C_2H_2 selective hydrogenation by controlling the composition and nanocluster size.

2. CALCULATION METHODS AND MODELS

2.1. Calculation Methods. In this study, all density functional theory (DFT) calculations are carried out in Dmol^3 program package and[38,39] the exchange-correlation functional is described using the generalized gradient approximation [GGA-Perdew−Burke−Ernzerhof (PBE)].[40,41] The effective core potentials (ECPs)[42] are employed to describe the interaction between the atomic core and electrons of metal, and all-electron basis set is used for other atoms. (The details about the choice of GGA-PBE and ECP are presented in the Supporting Information.) The double-numerical basis set with a polarization d-function (DNP)[43] is selected to expand the valence electron function. Moreover, the transition states (TSs) are obtained using the complete linear synchronous transit/quadratic synchronous transit method.[44,45] Furthermore, the transition state is confirmed by the frequency analysis with only one imaginary frequency, and the TS confirmation was used to confirm that the transition state was connected with the reactant and product.

The adsorption free energy (G_{ads}) is calculated by eq 1

$$G_{ads} = E_{total} + G_{total} - (E_{adsorbate} + G_{adsorbate} + E_{cluster} + G_{cluster}) \quad (1)$$

As shown in eq 1, E_{total} represents the energy of the total system and $E_{adsorbate}$ and $E_{cluster}$ represent the energy of the gaseous molecule and the nanocluster catalyst, respectively. $G_{adsorbate}$, $G_{cluster}$, and G_{total} are the Gibbs free energy of the gaseous species, the nanocluster, and the adsorbed system at 520 K, respectively.

The activation free energy (ΔG_a) and reaction free energy (ΔG) are defined according to eqs 2 and 3, respectively.

$$\Delta G_a = (E_{TS} + G_{TS}) - (E_R + G_R) \quad (2)$$

$$\Delta G = (E_P + G_P) - (E_R + G_R) \quad (3)$$

In eqs 2 and 3, E_P, E_R, and E_{TS} are the energies of reactants, products, and transition states, respectively, and G_R, G_{TS}, and

DOI: 10.1021/acs.jpcc.9b01757
J. Phys. Chem. C 2019, 123, 16107−16117

G_P represent the relative Gibbs free energies of reactants, transition states, and products at 520 K, respectively.

2.2. Computational Models. Since this study focuses on investigating the size and composition effect of core−shell catalysts on C_2H_4 selectivity and activity in C_2H_2 selective hydrogenation, the cluster models with different sizes are employed to simulate different sizes of core−shell catalysts rather than the periodic slab model, which is usually used to simulate the large-size bulk catalysts and cannot reflect the size effect such the small cluster size. Furthermore, previous studies have demonstrated that the M_{13}, M_{38}, and M_{55} cluster models of metal Cu or Pd with the corresponding diameters of about 5, 8, and 10 Å are the magic clusters, which exhibit excellent stability[26,46,47] and can be used to qualitatively represent the catalysts with different sizes. More importantly, among these cluster models, the larger-size M_{55} cluster model well exhibits the similar surface structure characteristics with the periodic Pd(111) or Cu(111) surface; as a result, the larger-size Pd_{55} or Cu_{55} cluster model in this study is regarded as the large-size Pd or Cu catalyst.

On the other hand, there are a number of low-coordinated sites such as the edges, corners, and kinks for the metal catalyst used in the experiment; however, the periodic slab model usually presents the only high-coordinated terrace sites of flat low-index surfaces, whereas the cluster models with different sizes can exhibit the sites with different coordination numbers. Among them, the number of low-coordinated sites increased significantly with the decrease in particle size, such as the M_{13} and M_{38} clusters, which cannot be properly reflected using the periodic slab models. Moreover, our previous studies[48] about C_2H_2 selective hydrogenation over the Pd-doped Cu bimetallic catalyst used the periodic slab model to simulate the core−shell Pd-doped Cu catalyst with the outermost layer Cu atoms of the periodic Cu(111) surface replaced by Pd atoms, which exhibits poor C_2H_4 selectivity; namely, the calculated results using the periodic slab model are not consistent with the experimental results that the Pd-doped Cu bimetallic catalyst significantly improve C_2H_4 selectivity. However, our results using the cluster model in this study show that the Pd-doped Cu bimetallic catalyst exhibits excellent C_2H_4 selectivity and activity.

On the basis of the above analysis, in this study, aiming at investigating the effects of composition and catalyst size on the catalytic performance of C_2H_2 selective hydrogenation, only the cluster model can reflect the structure characteristics of the core−shell catalysts with different sizes; moreover, it is reliable to employ the cluster model (M_{13}, M_{38}, and M_{55} cluster of metal Cu or Pd) to simulate the M@Pd and M@Cu core−shell catalyst and its size effect. Therefore, the M@Pd (M = Au, Ag, and Cu) core−shell nanoclusters with different sizes are constructed by replacing the core for different sizes of the pure Pd_{13}, Pd_{38}, and Pd_{55} clusters using the promoter Au, Ag, and Cu, respectively. Correspondingly, M@Cu (M = Au, Ag, and Pd) core−shell nanoclusters with different sizes are formed by replacing the core of single Cu clusters with different sizes (Cu_{13}, Cu_{38}, and Cu_{55}) using the promoter Au, Ag, and Pd, respectively; among them, our results show that both $M@Cu_{12}$ (M = Au and Ag) and $M_{13}@Cu_{42}$ (M = Au and Ag) clusters are not stable as the core−shell structure, which are not considered in this study. The corresponding stable structures of M@Pd (M = Au, Ag, and Cu) and M@Cu (M = Au, Ag, and Pd) nanoclusters with different sizes are shown in Figure 1. In addition, to identify the composition effects of core−shell catalysts, C_2H_2 selective hydrogenation over different sizes of single Cu and Pd nanocluster catalysts is also investigated in this study.

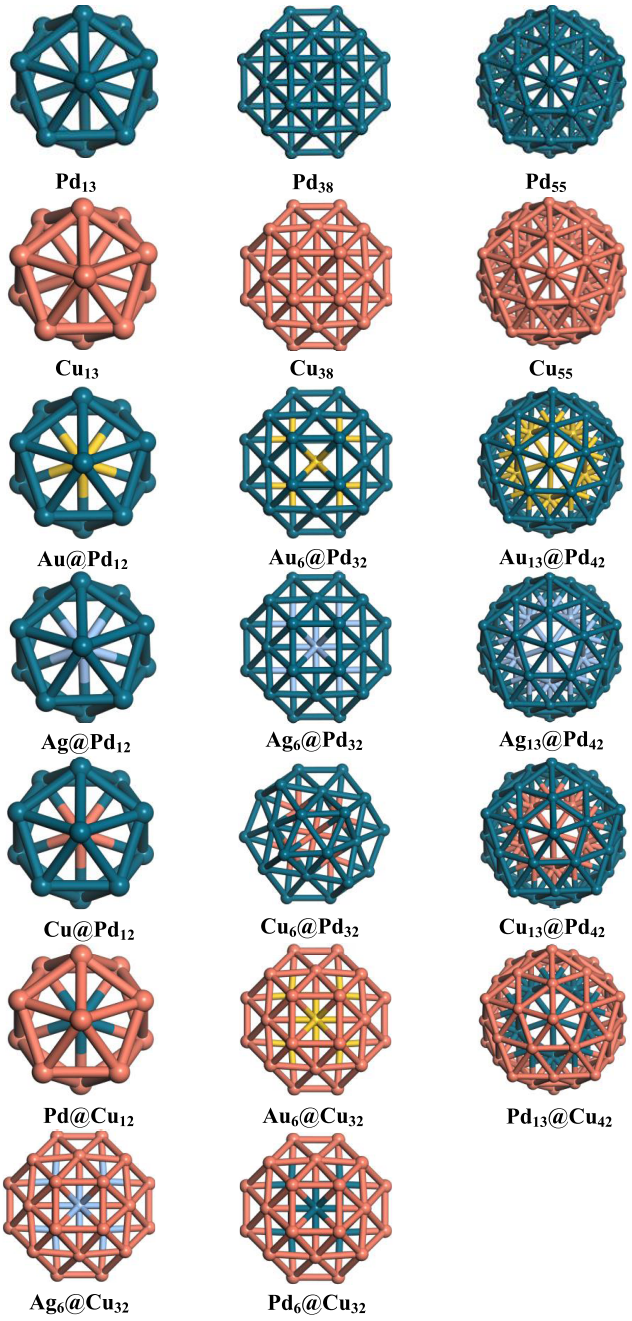

Figure 1. Stable structures for different sizes of M@Pd (M = Au, Ag, and Cu) and M@Cu (M = Au, Ag, and Pd) core−shell nanoclusters as well as the single Pd and Cu clusters.

3. RESULTS AND DISCUSSION

For C_2H_2 selective hydrogenation over Pd-based catalysts, the Pd hydride and Pd carbide may be formed during the reaction process and affect C_2H_4 selectivity.[49−51] Yang et al.[52] indicated that the presence of subsurface species (carbon and hydrogen) over the Pd catalyst affects the selectivity and activity of C_2H_4 formation. However, for CuPd alloy catalysts, Galipaud et al.[53] suggested that CuPd mixtures do not form a hydride phase for Cu/Pd bulk ratios of 0.5 and above. McCue et al.[20] found that

DOI: 10.1021/acs.jpcc.9b01757
J. Phys. Chem. C 2019, 123, 16107−16117

for the CuPd bimetallic catalysts, there is no Pd hydride for the Cu/Pd ratios of 100:1, 50:1, 25:1, and 10:1. Since this study focuses on investigating the size and composition effect of core−shell catalysts on C_2H_4 selectivity and activity in C_2H_2 selective hydrogenation, the effects of the Pd hydride and Pd carbide on the selectivity and activity of C_2H_4 formation have not been considered.

On the other hand, previous studies[20,48,52] have demonstrated that the higher temperature and H_2/C_2H_2 ratio can inhibit the formation of green oil, which will block the active site and result in the deactivation of the catalyst. Meanwhile, C_2H_2 selective hydrogenation over M@Cu catalysts is examined in this study, and only on the higher temperature (>473 K), metal Cu can act as the active component in C_2H_2 selective hydrogenation and exhibit high C_2H_4 selectivity.[19,21] Moreover, the present study will carry out the comparisons between M@Pd (M = Au, Ag, and Cu) and M@Cu (M = Au, Ag, and Pd) core−shell catalysts. Therefore, the high temperature of 520 K and high H_2/C_2H_2 ratio (10:1) were selected in this study, aiming at ignoring the effect of green oil formation on C_2H_2 selective hydrogenation over M@Pd and M@Cu core−shell catalysts; only C_2H_2 selective hydrogenation is considered, which can clearly identify the composition and size effects of M@Pd and M@Cu core−shell catalysts on the selectivity and activity of C_2H_4 formation. The 0.1, 0.01, and 0.89 partial pressures are used for H_2, C_2H_2, and C_2H_4 species, respectively, which are close to the real industrial environment.

On the basis of the above analysis, the effects of the Pd hydride and Pd carbide formation as well as the oligomer green oil on the selectivity and activity of C_2H_4 formation have not been considered, which can make us more clearly reveal the effect of the catalyst composition and size on the selectivity and activity of C_2H_2 selective hydrogenation. In addition, the effect of green oil formation will be further considered in our future work.

For the C_2H_2 selective hydrogenation (see Figure 2), there are three routes: C_2H_4 desorption route, C_2H_4 intermediate route, and $CHCH_3$ intermediate route. Among them, to remove the trace amount of C_2H_2 in C_2H_4 feedstock, C_2H_4 desorption route should be promoted, whereas both C_2H_4 intermediate and $CHCH_3$ intermediate routes should be inhibited.

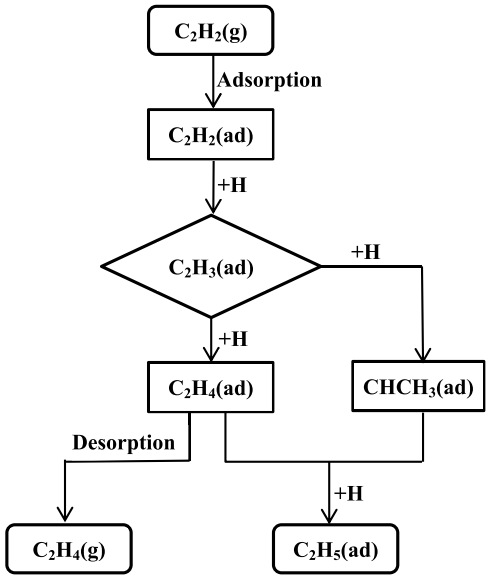

Figure 2. Reaction routes involved in C_2H_2 selective hydrogenation.

3.1. Evaluation Parameters of C_2H_4 Selectivity. In the industrial process of C_2H_2 selective hydrogenation, the content of C_2H_4 is nearly 89%, whereas the content of C_2H_2 is only 0.1−1%;[52] thus, only when the adsorption ability of C_2H_2 on the catalyst is much stronger than that of C_2H_4, the trace amount of C_2H_2 impurities in C_2H_4 feedstock can be preferentially adsorbed over the catalyst surface, which is in favor of C_2H_2 hydrogenation and its effective removal. As a result, the adsorption behaviors of C_2H_2 and C_2H_4 over M@Pd and M@Cu core−shell catalysts are first considered; as shown in Figure 3 and Table 1, the C_2H_4 adsorption abilities on all

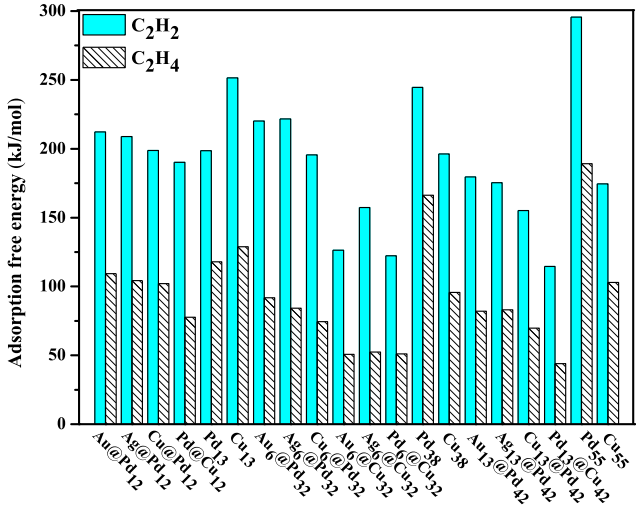

Figure 3. Adsorption free energies of C_2H_2 and C_2H_4 over different sizes of M@Pd (M = Au, Ag, and Cu) and M@Cu (M = Au, Ag, and Pd) core−shell nanoclusters as well as the single Pd and Cu clusters.

clusters are much weaker than that of C_2H_2, which is conducive for C_2H_2 selective hydrogenation. In addition, the stable structures of C_2H_x species adsorbed over M@Pd and M@Cu nanoclusters (see Figure S1) and the corresponding adsorption free energies (see Table 1) are calculated.

For the C_2H_2 selective hydrogenation, up to now, most of the theoretical studies[54−57] investigated all elementary steps involved in three reaction routes; then, the dominant reaction routes are determined by the overall free energies of three reaction routes; furthermore, when the C_2H_4 intermediate route is preferred, C_2H_4 selectivity was determined by the difference of overall free energies between C_2H_4 hydrogenation and C_2H_4 desorption routes. Second, recent studies by Xu et al.[58] proposed that the Gibbs free energy difference between the hydrogenation barrier and the desorption energy of C_2H_4 can be defined as the descriptor for C_2H_4 selectivity, and the $CHCH_3$ intermediate route is not considered. In fact, the $CHCH_3$ intermediate route can significantly affect C_2H_4 selectivity.

In this study, on the basis of the reported studies, a more reasonable method is proposed to evaluate C_2H_4 selectivity. First, the priority between the hydrogenation and desorption of C_2H_4 is considered. If the desorption of C_2H_4 is more preferred than its hydrogenation, then the preference between the $CHCH_3$ intermediate route and the C_2H_4 desorption route should be further investigated. When the C_2H_4 desorption

DOI: 10.1021/acs.jpcc.9b01757
J. Phys. Chem. C 2019, 123, 16107−16117

Table 1. Adsorption Free Energies of C_2H_2 and C_2H_4 over Different Sizes of M@Pd (M = Au, Ag, and Cu) and M@Cu (M = Au, Ag, and Pd) Core−Shell Catalysts as Well as the Single Pd and Cu Clusters at 520 K

	adsorption free energies (G_{ads}/kJ mol^{-1})				
clusters	C_2H_2	C_2H_3	C_2H_4	$CHCH_3$	C_2H_5
$Au@Pd_{12}$	−212.2	−339.9	−109.3	−430.5	−175.8
$Ag@Pd_{12}$	−208.8	−342.8	−104.3	−350.1	−177.1
$Cu@Pd_{12}$	−198.7	−340.0	−102.0	−446.3	−171.7
Pd_{13}	−198.6	−311.6	−117.9	−403.8	−224.1
$Au_6@Pd_{32}$	−220.1	−431.1	−91.8	−515.0	−173.9
$Ag_6@Pd_{32}$	−221.6	−443.6	−84.2	−507.9	−176.4
$Cu_6@Pd_{32}$	−195.6	−567.3	−74.4	−588.1	−173.7
Pd_{38}	−244.6	−402.0	−166.3	−472.3	−295.3
$Au_{13}@Pd_{42}$	−179.6	−273.7	−82.1	−348.9	−156.7
$Ag_{13}@Pd_{42}$	−175.4	−263.0	−83.0	−355.5	−166.1
$Cu_{13}@Pd_{42}$	−155.1	−243.5	−69.7	−333.2	−155.9
Pd_{55}	−295.6	−396.6	−189.2	−487.6	−301.6
$Pd@Cu_{12}$	−190.1	−399.9	−77.7	−460.7	−200.4
Cu_{13}	−251.5	−331.6	−128.9	−250.4	−255.4
$Au_6@Cu_{32}$	−126.4	−265.1	−50.7	−311.4	−174.4
$Ag_6@Cu_{32}$	−157.4	−258.2	−52.4	−311.0	−164.0
$Pd_6@Cu_{32}$	−122.3	−241.7	−51.0	−313.0	−157.2
Cu_{38}	−196.3	−310.9	−95.6	−381.6	−238.7
$Pd_{13}@Cu_{42}$	−114.5	−276.3	−44.0	−301.7	−140.8
Cu_{55}	−174.5	−298.3	−103.0	−385.9	−245.1

route is preferred than the $CHCH_3$ intermediate route, the catalyst exhibits better C_2H_4 selectivity; otherwise, the catalyst shows poor C_2H_4 selectivity. On the other hand, if C_2H_4 is preferred for hydrogenation to form C_2H_5 rather than desorption to gaseous C_2H_4, then the catalyst exhibits poor C_2H_4 selectivity, and the effects of the $CHCH_3$ intermediate route on the C_2H_4 selectivity are not considered.

C_2H_4 selectivity is evaluated by the energy difference between the hydrogenation of C_2H_4 and the adsorption of C_2H_4, which is calculated using eq 4[54,58−60]

$$G_{sel} = \Delta G_a - |G_{ads}| \quad (4)$$

As shown in eq 4, ΔG_a corresponds to the activation free energy of hydrogenation routes (the C_2H_4 intermediate or $CHCH_3$ intermediate route) and G_{ads} corresponds to the activation free energy of the C_2H_4 adsorption route; when the value of G_{sel} is more positive and larger, which represents that C_2H_4 more easily undergoes desorption to form gaseous C_2H_4 instead of ethane formed by C_2H_4 successive hydrogenation, the catalyst exhibits good C_2H_4 selectivity.

3.2. C_2H_2 Selective Hydrogenation on M@Pd (M = Au, Ag, and Cu) Clusters. For the $M@Pd_{12}$ (M = Au, Ag, and Cu) clusters, on $Au@Pd_{12}$ (see Figure 4a), the desorption of adsorbed C_2H_4 to gaseous C_2H_4 is slightly advantageous than the hydrogenation of C_2H_4 in terms of kinetics (109.3 vs 113.3 kJ mol^{-1}). Meanwhile, the $CHCH_3$ intermediate route is much difficult than the C_2H_4 desorption route in terms of kinetics (223.1 vs 166.8 kJ mol^{-1}, see Figure S2); as a result, the C_2H_4 desorption route is an advantageous way with the C_2H_4 selectivity (G_{sel}) of 4.0 kJ mol^{-1}. Similarly, on $Ag@Pd_{12}$ (Figure 4b), the C_2H_4 desorption route is the most advantageous with the G_{sel} of 8.7 kJ mol^{-1}, and the $CHCH_3$ intermediate route is much difficult than the C_2H_4 desorption route (197.2 vs 112.8 kJ mol^{-1}, see Figure S3). However, on $Cu@Pd_{12}$ clusters, the hydrogenation of C_2H_4 is more

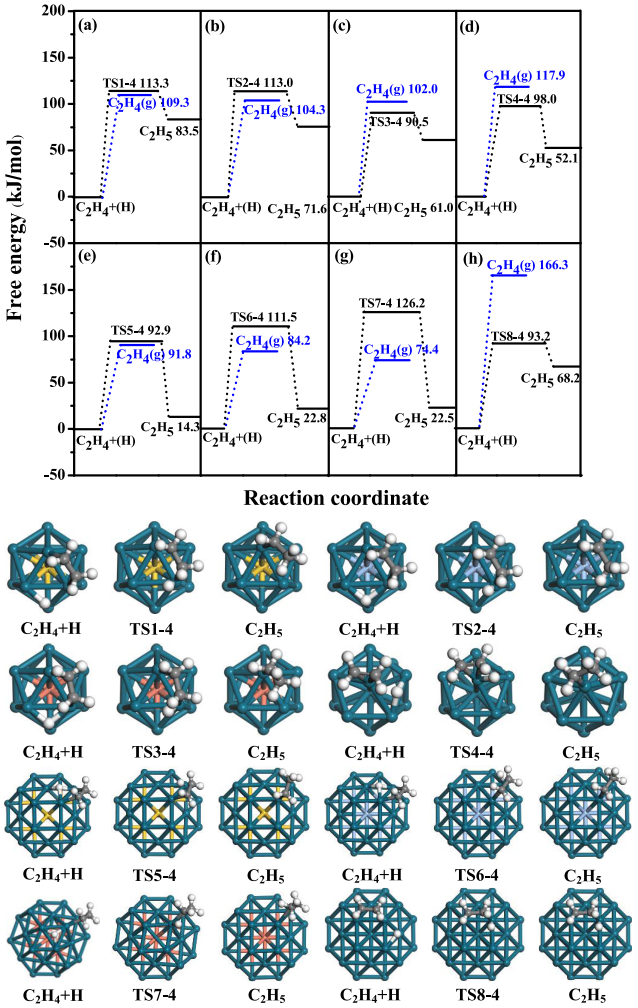

Figure 4. Potential energy profiles of C_2H_4 hydrogenation and C_2H_4 desorption over the (a) $Au@Pd_{12}$, (b) $Ag@Pd_{12}$, (c) $Cu@Pd_{12}$, (d) single Pd_{13}, (e) $Au_6@Pd_3$, (f) $Ag_6@Pd_{32}$, (g) $Cu_6@Pd_{32}$, and (h) single Pd_{38} clusters.

advantageous than its desorption (90.5 vs 102.0 kJ mol^{-1}, see Figure 4c) to present poor C_2H_4 selectivity with the G_{sel} of −11.5 kJ mol^{-1}. In addition, the hydrogenation of C_2H_4 is easier than the desorption of C_2H_4 to gaseous C_2H_4 (98.0 vs 117.9 kJ mol^{-1}) on the single Pd_{13} cluster (Figure 4d) to exhibit poor C_2H_4 selectivity with the G_{sel} of −19.9 kJ mol^{-1}. Hence, $M@Pd_{12}$ (M = Au, Ag, and Cu) clusters slightly improve C_2H_4 selectivity compared to the single Pd_{13} cluster.

As for the $M_6@Pd_{32}$ (M = Au, Ag, and Cu) clusters, as shown in Figure 4e−g, the C_2H_4 desorption route is advantageous than the C_2H_4 intermediate route (91.8 vs 92.9, 84.2 vs 111.5, and 74.4 vs 126.2 kJ mol^{-1}, respectively). Meanwhile, the $CHCH_3$ intermediate route is also difficult than the C_2H_4 desorption route (Figures S4−S6). Compared to the single Pd_{38} cluster with the G_{sel} of −73.1 kJ mol^{-1} (Figure 4h), $M_6@Pd_{32}$ (M = Au, Ag, and Cu) clusters present better C_2H_4 selectivity (the G_{sel} of 1.1, 27.3, and 51.8 kJ mol^{-1}, respectively); in particular, $Cu_6@Pd_{32}$ clusters exhibit the best C_2H_4 selectivity.

For the $M_{13}@Pd_{42}$ (M = Au, Ag, and Cu) clusters, as shown in Figure 5a−c, the C_2H_4 desorption route is more advantageous than the C_2H_4 intermediate route (82.1 vs 118.2, 83.0 vs 121.3, and 69.7 vs 137.6 kJ mol^{-1}, respectively);

DOI: 10.1021/acs.jpcc.9b01757
J. Phys. Chem. C 2019, 123, 16107−16117

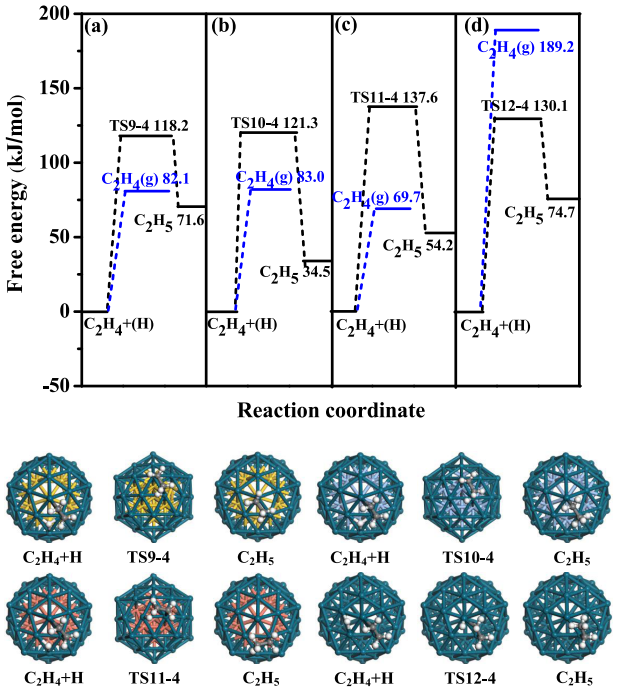

Figure 5. Potential energy profiles of C_2H_4 hydrogenation and C_2H_4 desorption over the (a) $Au_{13}@Pd_{42}$, (b) $Ag_{13}@Pd_{42}$, (c) $Cu_{134}@Pd_{42}$, and (d) single Pd_{55} clusters.

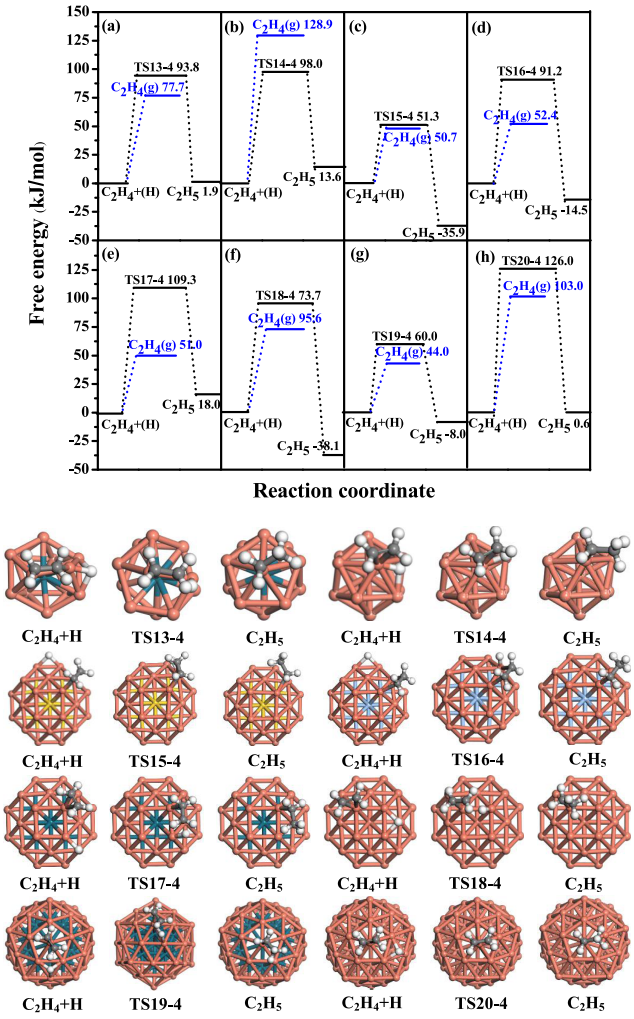

Figure 6. Potential energy profiles of C_2H_4 hydrogenation and C_2H_4 desorption over the (a) $Pd@Cu_{12}$, (b) single Cu_{13}, (c) $Au_6@Cu_{32}$, (d) $Ag_6@Cu_{32}$, (e) $Pd_6@Cu_{32}$, (f) single Cu_{38}, (g) $Pd_{13}@Cu_{42}$, and (h) single Cu_{55} clusters.

moreover, the $CHCH_3$ intermediate route is unfavorable in comparison with the C_2H_4 desorption route (202.4 vs 143.4, 220.2 vs 156.2, and 120.4 vs 97.9 kJ mol^{-1}, respectively, see Figures S7–S9). As a result, $M_{13}@Pd_{42}$ (M = Au, Ag, and Cu) clusters exhibit higher C_2H_4 selectivity (the G_{sel} of 36.1, 38.3, and 67.9 kJ mol^{-1}, respectively) compared to the single Pd_{55} cluster with the G_{sel} of −59.1 kJ mol^{-1} (see Figure 5d); especially, $Cu_{13}@Pd_{42}$ cluster shows excellent C_2H_4 selectivity.

3.3. C_2H_2 Selective Hydrogenation on M@Cu (M = Au, Ag, and Pd) Clusters. As mentioned in Section 2.2, both $M@Cu_{12}$ (M = Au and Ag) and $M_{13}@Cu_{42}$ (M = Au and Ag) clusters are not stable as the core–shell structure, which are not considered in this study.

For the $Pd@Cu_{12}$ cluster, the desorption of C_2H_4 is much easier among the three routes (Figures 6a and S10) with the G_{sel} of 16.1 kJ mol^{-1}. The single Cu_{13} cluster shows poor C_2H_4 selectivity with the G_{sel} of −30.9 kJ mol^{-1} (Figure 6b). Thus, the $Pd@Cu_{12}$ cluster presents better C_2H_4 selectivity compared to the single Cu_{13} cluster.

For $M_6@Cu_{32}$ (M = Au, Ag, and Pd) clusters, the hydrogenation of C_2H_4 and C_2H_4 desorption routes are energetically competitive (51.3 vs 50.7 kJ mol^{-1}) on $Au_6@Cu_{32}$ clusters (Figures 6c and S11) with the small G_{sel} of 0.6 kJ mol^{-1}. For the $Ag_6@Cu_{32}$ and $Pd_6@Cu_{32}$ clusters (Figure 6d,e), the C_2H_4 desorption route is the most optimal compared to other two routes (Figures S12 and S13); both clusters exhibit good C_2H_4 selectivity with the G_{sel} of 38.8 and 58.3 kJ mol^{-1}, respectively. Hence, $M_6@Cu_{32}$ (M = Au, Ag, and Pd) clusters effectively improve C_2H_4 selectivity compared to the single Cu_{38} cluster (Figure 6f) with the G_{sel} of −21.9 kJ mol^{-1}.

$Pd_{13}@Cu_{42}$ clusters (Figures 6g and S14) exhibit good C_2H_4 selectivity with the G_{sel} of 16.0 kJ mol^{-1}. However, compared to the single Cu_{55} cluster (Figures 6h and S15) with the C_2H_4 selectivity of 23.0 kJ mol^{-1}, $Pd_{13}@Cu_{42}$ clusters exhibit poor C_2H_4 selectivity.

3.4. General Discussion. Based on the above analysis, different sizes of M@Pd (M = Au, Ag, and Cu) and M@Cu (M = Au, Ag, and Pd) core–shell nanoclusters with good C_2H_4 selectivity were screened; then, the formation rate of C_2H_4 was further investigated to describe the catalytic activity. Meanwhile, the formation rate of C_2H_4 over the corresponding sizes of single Pd and Cu clusters was considered as a reference. The formation rate of C_2H_4 was calculated through the two-step model proposed by Cheng et al.[61,62] (The detailed descriptions are presented in the Supporting Information.) The formation rate of C_2H_4 was calculated according to eq 5

$$r = \frac{k_B T}{h} \frac{\left(1 - \frac{P_P}{P_R} e^{\Delta G/RT}\right)}{\frac{P^0}{P_R} e^{G_R^{ad} - G_R^{de} + G_P^{de}/RT} + e^{G_P^{de}/RT}} \quad (5)$$

According to eq 5, the major parameters for the formation rate of C_2H_4 are G_R^{ad}, G_R^{de}, and G_P^{de}, and we can obtain the values of G_R^{de} and G_P^{de} from the potential energy profiles of C_2H_2 selective hydrogenation to form C_2H_4 (Figure 7). On the other hand, previous studies suggested that the TS_R (R = C_2H_2

DOI: 10.1021/acs.jpcc.9b01757
J. Phys. Chem. C 2019, 123, 16107−16117

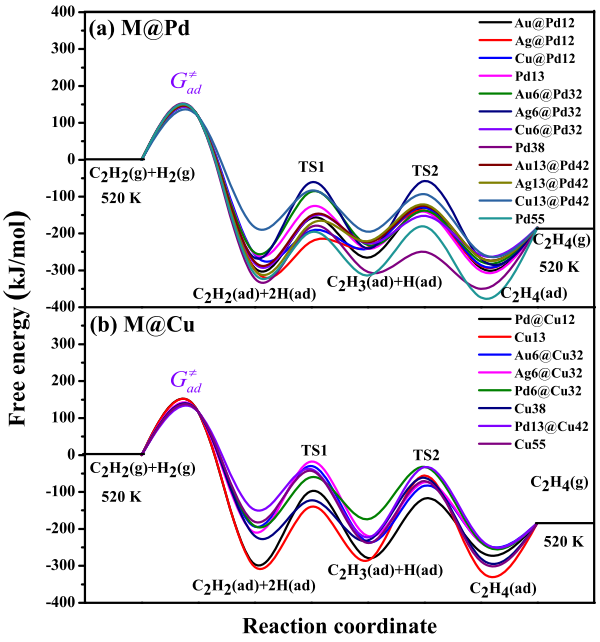

Figure 7. Free energy profiles of the selective hydrogenation of C_2H_2 to C_2H_4 on different sizes of M@Pd (M = Au, Ag, and Cu), M@Cu (M = Au, Ag, and Pd), and the single Pd and Cu clusters.

and H_2) is used to describe the value of G_R^{ad}; in this study, at the reaction temperature of T = 520 K, $TS_{C_2H_2}$ = 117.6 kJ mol^{-1} and TS_{H_2} = 76.3 kJ mol^{-1}, indicating that C_2H_2 has higher adsorption free energy than H_2. Thus, the adsorption free energy of C_2H_2 (117.6 kJ mol^{-1}) is selected as the limiting adsorption barrier of the reactants. The calculated rates of C_2H_4 formation over different sizes of core−shell catalysts with good C_2H_4 selectivity are listed in Table 2.

3.4.1. Effects of Core and Shell Compositions on C_2H_4 Selectivity and Activity. As shown in Figure 8a, for different sizes of M@Pd (M = Au, Ag, and Cu) nanoclusters, M@Pd_{12}

Table 2. Values of $G_R^{ad} - G_R^{de} + G_P^{de}$, G_P^{de} (kJ mol^{-1}) and Reaction Rate (r/s^{-1} site^{-1}) at 520 K on Different Clusters

clusters	$G_R^{ad} - G_R^{de} + G_P^{de}$	G_P^{de}	r
Au@Pd_{12}	−129.5	164.0	3.64×10^{-4}
Ag@Pd_{12}	−137.8	160.4	8.33×10^{-4}
Cu@Pd_{12}	−187.9	128.1	1.47×10^{0}
Pd_{13}	−126.3	128.6	1.30×10^{0}
Au_6@Pd_{32}	−86.2	165.8	2.40×10^{-4}
Ag_6@Pd_{32}	−57.7	208.7	1.18×10^{-8}
Cu_6@Pd_{32}	−152.0	129.4	1.09×10^{0}
Pd_{38}	−181.9	140.3	8.71×10^{-2}
Au_{13}@Pd_{42}	−124.8	152.0	5.83×10^{-3}
Ag_{13}@Pd_{42}	−120.9	178.3	1.33×10^{-5}
Cu_{13}@Pd_{42}	−83.1	99.8	1.02×10^{3}
Pd_{55}	−180.9	129.0	1.19×10^{0}
Pd@Cu_{12}	−97.5	197.8	1.46×10^{-7}
Cu_{13}	−55.1	247.1	1.63×10^{-12}
Au_6@Cu_{32}	29.7	222.8	4.50×10^{-10}
Ag_6@Cu_{32}	22.2	231.5	6.26×10^{-7}
Pd_6@Cu_{32}	−32.4	159.5	1.03×10^{-3}
Cu_{38}	−61.5	157.1	1.79×10^{-3}
Pd_{13}@Cu_{42}	−32.5	115.8	2.53×10^{1}
Cu_{55}	−42.8	138.1	1.45×10^{-1}

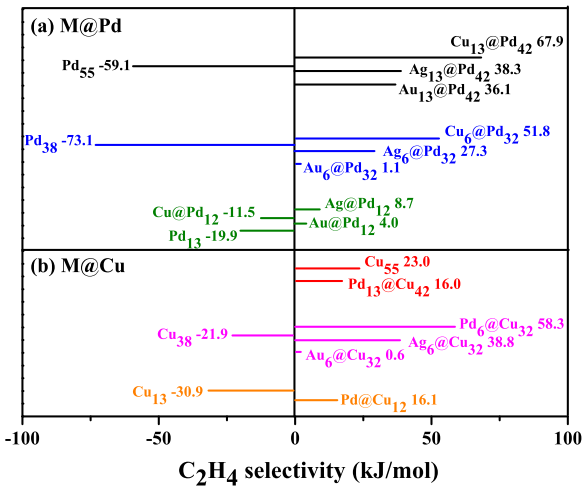

Figure 8. C_2H_4 selectivity (G_{sel}) over different sizes of M@Pd (M = Au, Ag, and Cu) and M@Cu (M = Au, Ag, and Pd), and the single Pd and Cu clusters at 520 K.

clusters show poor C_2H_4 selectivity compared to M_6@Pd_{32} and M_{13}@Pd_{42} clusters, and C_2H_4 selectivity (G_{sel}/kJ mol^{-1}) over M_6@Pd_{32} and M_{13}@Pd_{42} clusters follows the order: Pd_{38} (−73.1) < Au_6@Pd_{32} (1.1) < Ag_6@Pd_{32} (27.3) < Cu_6@Pd_{32} (51.8), and Pd_{55} (−59.1) < Au_{13}@Pd_{42} (36.1) < Ag_{13}@Pd_{42} (38.3) < Cu_{13}@Pd_{42} (67.9); namely, C_2H_4 selectivity (G_{sel}/kJ mol^{-1}) over M_6@Pd_{32} and M_{13}@Pd_{42} clusters follows the order: Pd < Au@Pd < Ag@Pd < Cu@Pd. Furthermore, the formation rates of C_2H_4 (r/s^{-1} site^{-1}) follow the order (see Table 2): Ag@Pd (1.18×10^{-8}) < Au@Pd (2.40×10^{-4}) < Pd (8.71×10^{-2}) < Cu@Pd (1.09×10^{0}) for M_6@Pd_{32} clusters, Ag@Pd (1.33×10^{-5}) < Au@Pd (5.83×10^{-3}) < Pd (1.19×10^{0}) < Cu@Pd (1.02×10^{3}) for M_{13}@Pd_{42} clusters. The above results show that compared to the single Pd cluster, both Au@Pd and Ag@Pd clusters effectively improve C_2H_4 selectivity; however, these types of clusters decrease the catalytic activity of C_2H_4 formation. This result is consistent with the experimental results by Khan et al.;[3] they investigated the catalytic performance of the Al_2O_3-supported Pd−Ag catalyst for C_2H_2 selective hydrogenation, indicating that the modification of Ag improves C_2H_4 selectivity but decreases the activity of C_2H_4 formation. Moreover, Sárkány et al.[10] suggested that the modification of Au for the Pd catalyst decreased the catalytic activity and improved C_2H_4 selectivity. As a result, only the Cu@Pd nanoclusters significantly not only improve C_2H_4 selectivity but also the catalytic activity of C_2H_4 formation. Therefore, for the M@Pd core−shell catalyst, the core M composition affects not only C_2H_4 selectivity but also the catalytic activity of C_2H_4 formation in C_2H_2 selective hydrogenation, in which the metal Cu as the core for M@Pd core−shell catalysts presents the excellent selectivity and activity of C_2H_4 formation than Au and Ag as the core.

For different sizes of M@Cu (M = Au, Ag, and Pd) clusters, as mentioned above, the M@Cu_{12} (M = Au, and Ag) and M_{13}@Cu_{42} (M = Au and Ag) nanoclusters are not stable as the core−shell structure. Hence, when the core composition of M@Cu nanoclusters is Au and Ag, the nanoclusters shows poor stability, whereas different sizes of Pd@Cu nanoclusters can exist in the form of stable structures. As shown in Figure 8b, for M@Cu_{12}, the Pd@Cu_{12} nanocluster shows better C_2H_4 selectivity than the single Cu_{13} cluster (16.1 vs −30.9 kJ mol^{-1}); moreover, the formation rate of C_2H_4 (r/s^{-1} site^{-1})

DOI: 10.1021/acs.jpcc.9b01757
J. Phys. Chem. C 2019, 123, 16107−16117

(see Table 2) over Pd@Cu_{12} nanoclusters (1.46×10^{-7}) is higher than that of single Cu_{13} clusters (1.63×10^{-12}), suggesting that the Pd@Cu_{12} nanocluster improves C_2H_4 selectivity and catalytic activity. For M_6@Cu_{32} nanoclusters, the order of C_2H_4 selectivity (G_{sel}/kJ mol^{-1}) is as follows: Cu_{38} (−21.9) < Au_6@Cu_{32} (0.6) < Ag_6@Cu_{32} (38.8) < Pd_6@Cu_{32} (58.3), and the formation rates of C_2H_4 (r/s^{-1} $site^{-1}$) follow the order: Au_6@Cu_{32} (4.50×10^{-10}) < Ag_6@Cu_{32} (6.26×10^{-7}) < Pd_6@Cu_{32} (1.03×10^{-3}) ≈ Cu_{38} (1.79×10^{-3}), indicating that compared to the single Cu_{38} cluster, the M_6@Cu_{32} (M = Au, Ag, and Pd) nanoclusters improve only C_2H_4 selectivity, whereas they do not enhance the catalytic activity of C_2H_4 formation. Moreover, for M_{13}@Cu_{42}, the Pd_{13}@Cu_{42} nanocluster cannot improve C_2H_4 selectivity compared to the single Cu_{55} cluster (16.0 vs 23.0 kJ mol^{-1}). Thus, the core M composition of M@Cu core−shell catalysts alters C_2H_4 selectivity and catalytic activity in the selective hydrogenation of C_2H_2. In the M@Cu core−shell catalyst, the metal Pd as the core presents better C_2H_4 selectivity and catalytic activity than the metals Au or Ag as the core. However, compared to the single Cu clusters, the Pd@Cu nanoclusters with different sizes cannot effectively improve C_2H_4 selectivity or catalytic activity, which is not suitable for C_2H_2 selective hydrogenation.

More importantly, as mentioned above, different sizes of Pd@Cu nanoclusters show poor C_2H_4 selectivity and activity than the corresponding sizes of Cu@Pd nanoclusters; this result further shows that the shell composition of core−shell catalysts exhibits a great influence on C_2H_4 selectivity and catalytic activity, in which the metal Pd as the shell shows better C_2H_4 selectivity and catalytic activity than the metal Cu as the shell. Thus, both the core and shell composition of the core−shell catalyst affect C_2H_4 selectivity and catalytic activity. Among them, the core−shell catalysts with the metal Cu as the core and the Pd as the shell (Cu@Pd) are suitable catalysts to fundamentally improve C_2H_4 selectivity and activity in C_2H_2 selective hydrogenation.

3.4.2. Cluster Size Effects of Core−Shell Catalysts on C_2H_4 Selectivity and Activity. As mentioned above, the Cu@Pd catalysts with Pd as the shell and Cu as the core exhibit excellent C_2H_4 selectivity and catalytic activity. For the different sizes of Cu@Pd core−shell catalysts, the order of C_2H_4 selectivity (G_{sel}/kJ mol^{-1}) is as follows: Cu@Pd_{12} (−11.5) < Cu_6@Pd_{32} (51.8) < Cu_{13}@Pd_{42} (67.9); meanwhile, the formation rates of C_2H_4 (r/s^{-1} $site^{-1}$) follow the order: Cu@Pd_{12} (1.46×10^{-7}) < Cu_6@Pd_{32} (1.09×10^{0}) < Cu_{13}@Pd_{42} (1.02×10^{3}). Thus, C_2H_4 selectivity and catalytic activity increase with the increasing size of Cu@Pd nanoclusters, and the large-size Cu_{13}@Pd_{42} nanocluster exhibits the best C_2H_4 selectivity and activity, which is conducive to the selective hydrogenation of C_2H_2. Namely, in the experimental preparation of Cu@Pd core−shell catalysts, controlling the particle size of the catalyst in a larger size range is conducive to enhance C_2H_4 selectivity and catalytic activity in the selective hydrogenation of C_2H_2.

3.4.3. Electronic Structure Analysis. On the basis of the above analysis, different sizes of Cu@Pd nanoclusters exhibit better C_2H_4 selectivity and catalytic activity than those of Au@Pd and Ag@Pd nanoclusters. Thus, the projected density of states (pDOS) of M@Pd (M = Au, Ag, and Cu) nanoclusters with different sizes are calculated to illustrate the microscopic reasons about the effects of compositions and nanocluster size on the catalytic activity of C_2H_2 selective hydrogenation, and the d-centers of different nanoclusters are shown in Figure 9.

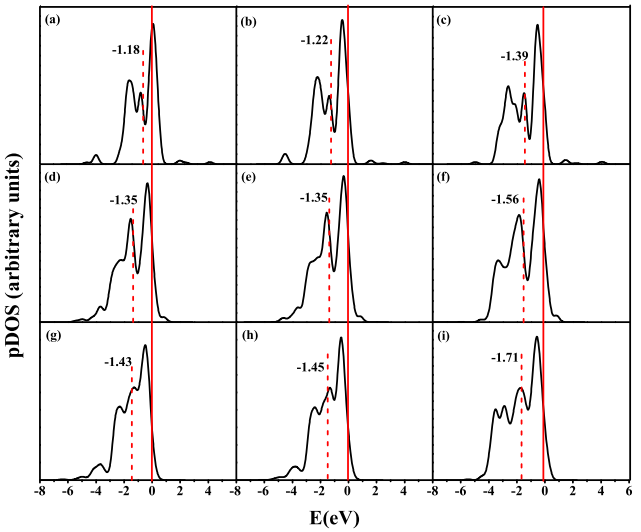

Figure 9. Projected density of states (pDOS) plots of the d-orbitals for the outer layer Pd atoms of (a) Au@Pd_{12}, (b) Ag@Pd_{12}, (c) Cu@Pd_{12}, (d) Au_6@Pd_{32}, (e) Ag_6@Pd_{32}, (f) Cu_6@Pd_{32}, (g) Au_{13}@Pd_{42}, (h) Ag_{13}@Pd_{42}, and (i) Cu_{13}@Pd_{42} nanoclusters.

According to previous results,[63−65] for the C_2H_x hydrogenation reaction, the activation of the C−H bond mainly depends on the electron backdonation to the antibonding σCH* orbital, and when the d-band center of the metal surface is far away from the Fermi level, the metal surface is more active for hydrogenation and C_2H_x hydrogenation should have high activity.

For the M@Pd_{12} (M = Au, Ag, and Cu) clusters, as shown in Figure 9a−c, the d-band center (eV) follows the order: Cu@Pd_{12} (−1.39) < Ag@Pd_{12} (−1.22) < Au@Pd_{12} (−1.18); the results show that the Cu@Pd_{12} cluster is far from the Fermi level than Au@Pd_{12} and Ag@Pd_{12} clusters. As a result, the formation rates of C_2H_4 (s^{-1} $site^{-1}$) over M@Pd_{12} clusters follow the order: Au@Pd_{12} (3.64×10^{-4}) ≈ Ag@Pd_{12} (8.33×10^{-4}) < Cu@Pd_{12} (1.47×10^{0}). Interestingly, the same results are observed on the M_6@Pd_{32} and M_{13}@Pd_{42} clusters (Figure 9d−i); in general, the Cu@Pd nanoclusters are far away from the Fermi level than the Au@Pd and Ag@Pd clusters. Cu@Pd clusters exhibit the highest catalytic activity for C_2H_4 formation. Therefore, the core composition of core−shell catalysts changes the d-band center of the shell metal and further affects the catalytic activity of C_2H_4 formation. When metal Cu acts as the core for M@Pd catalysts, the d-band center of shell Pd atoms is far from the Fermi level, so they show the best catalytic activity for C_2H_4 formation.

Moreover, for different sizes of Cu@Pd nanoclusters, as shown in Figure 9c,f,i, the order of d-band center (eV) is as follows: Cu_{13}@Pd_{42} (−1.71) < Cu_6@Pd_{32} (−1.56) < Cu@Pd_{12} (−1.39), suggesting that the d-band center of shell Pd atoms in Cu@Pd nanoclusters is also far away from the Fermi level with the increase in the nanocluster size. Thus, as mentioned above, the large-size Cu_{13}@Pd_{42} (1.02×10^{3} s^{-1} $site^{-1}$) nanocluster exhibits the best catalytic activity for C_2H_4 formation than both Cu@Pd_{12} (1.47×10^{0} s^{-1} $site^{-1}$) and Cu_6@Pd_{32} (1.09×10^{0} s^{-1} $site^{-1}$) nanoclusters.

4. CONCLUSIONS

In this study, C_2H_2 selective hydrogenation on different compositions of M@Pd (M = Au, Ag, and Cu) and M@Cu (M

DOI: 10.1021/acs.jpcc.9b01757
J. Phys. Chem. C 2019, 123, 16107−16117

= Au, Ag, and Pd) nanoclusters with different sizes has been investigated, which aims at identifying the effects of the composition and the nanocluster size on the selectivity and activity of C_2H_4 formation. The results show that the metal Cu as the core of M@Pd core−shell catalysts can effectively improve C_2H_4 selectivity and activity than Au and Ag; similarly, for M@Cu (M = Au, Ag, and Pd) nanoclusters, the metal Pd as the core of M@Cu core−shell catalysts exhibits the best C_2H_4 selectivity and activity than that of Au and Ag; moreover, compared to Cu@Pd nanoclusters, Pd@Cu nanoclusters show poor selectivity and activity of C_2H_4 formation. Thus, the shell and core composition of core−shell catalysts have a great effect on the catalytic performance; the Cu@Pd core−shell catalysts with Cu as the core and Pd as the shell are the most advantageous to improve the selectivity and activity of C_2H_4 formation, which are suitable catalysts for C_2H_2 selective hydrogenation. On the other hand, with the increase in the size of Cu@Pd nanoclusters, the selectivity and activity of C_2H_4 formation over Cu@Pd nanoclusters increase. $Cu_{13}@Pd_{42}$ nanoclusters exhibit the best activity of C_2H_4 formation, which is attributed to changes in the *d*-band center of the shell metal due to the core composition of core−shell catalysts, and further affect the catalytic activity of C_2H_4 formation. The d-band center of shell Pd atoms is far from the Fermi level, so they show the best catalytic activity of C_2H_4 formation. Therefore, for the preparation of Cu@Pd core−shell catalysts in C_2H_2 selective hydrogenation, it is expected to have the particle size of core−shell catalysts within a larger size range, which is conducive to enhance the selectivity and activity of C_2H_4 formation.

■ ASSOCIATED CONTENT

Supporting Information

The Supporting Information is available free of charge on the ACS Publications website at DOI: 10.1021/acs.jpcc.9b01757.

Detailed descriptions about the choice of the functional (PBE) and the core treatment parameter (ECP); all of the stable adsorption configurations of C_2H_x (x = 2−5) species; structures of initial states, transition states, and final states involved in C_2H_2 selective hydrogenation over different compositions and sizes of M@Pd and M@Cu core−shell catalysts; and two-step model of C_2H_4 formation (PDF)

■ AUTHOR INFORMATION

Corresponding Authors

*E-mail: wangbaojun@tyut.edu.cn, wbj@tyut.edu.cn (B.W.).
*E-mail: mfan@uwyo.edu (M.F.).

ORCID

Baojun Wang: 0000-0002-9069-6720
Maohong Fan: 0000-0003-1334-7292

Notes

The authors declare no competing financial interest.

■ ACKNOWLEDGMENTS

This work is financially supported by the National Natural Science Foundation of China (No. 21776193), the Key projects of the National Natural Science Foundation of China (No. 21736007) and the Top Young Innovative Talents of Shanxi, and U.S. NSF-sponsored NCAR-Wyoming Supercomputing Center (NWSC).

■ REFERENCES

(1) Yang, J.; Lv, C. Q.; Guo, Y.; Wang, G. C. A DFT + U Study of Acetylene Selective Hydrogenation on Oxygen Defective Anatase (101) and Rutile (110) TiO_2 Supported Pd_4 Cluster. *J. Chem. Phys.* **2012**, *136*, No. 104107.

(2) Sheth, P. A.; Neurock, M.; Smith, C. M. A First-Principles Analysis of Acetylene Hydrogenation over Pd(111). *J. Phys. Chem. B* **2003**, *107*, 2009−2017.

(3) Khan, N. A.; Shaikhutdinov, S.; Freund, H. J. Acetylene and Ethylene Hydrogenation on Alumina Supported Pd-Ag Model Catalysts. *Catal. Lett.* **2006**, *108*, 159−164.

(4) Zhang, J.; Sui, Z. J.; Zhu, Y. A.; Chen, D.; Zhou, X. G.; Yuan, W. K. Composition of the Green oil in Hydrogenation of Acetylene over a Commercial Pd-Ag/Al_2O_3 Catalyst. *Chem. Eng. Technol.* **2016**, *39*, 865−873.

(5) Ngamsom, B.; Bogdanchikova, N.; Borja, M. A.; Praserthdam, P. Characterisations of Pd−Ag/Al_2O_3 Catalysts for Selective Acetylene Hydrogenation: Effect of Pretreatment with NO and N_2O. *Catal. Commun.* **2004**, *5*, 243−248.

(6) Osswald, J.; Kovnir, K.; Armbrüster, M.; Giedigkeit, R.; Jentoft, R. E.; Wild, U.; Grin, Y.; Schlögl, R. Palladium−Gallium Intermetallic Compounds for the Selective Hydrogenation of Acetylene: Part II: Surface Characterization and Catalytic Performance. *J. Catal.* **2008**, *258*, 219−227.

(7) Kim, S. K.; Lee, J. H.; Ahn, I. Y.; Kim, W. J.; Moon, S. H. Performance of Cu-Promoted Pd Catalysts Prepared by Adding Cu Using a Surface Redox Method in Acetylene Hydrogenation. *Appl. Catal., A* **2011**, *401*, 12−19.

(8) Choudhary, T. V.; Sivadinarayana, C.; Datye, A. K.; Kumar, D.; Goodman, D. W. Acetylene Hydrogenation on Au-Based Catalysts. *Catal. Lett.* **2003**, *86*, 1−8.

(9) Sárkány, A.; Geszti, O.; Sáfrán, G. Preparation of Pd_{shell}−Au_{core}/SiO_2 Catalyst and Catalytic Activity for Acetylene Hydrogenation. *Appl. Catal., A* **2008**, *350*, 157−163.

(10) Sárkány, A.; Horváth, A.; Beck, A. Hydrogenation of Acetylene over low Loaded Pd and Pd-Au/SiO_2 Catalysts. *Appl. Catal., A* **2002**, *229*, 117−125.

(11) Pei, G. X.; Liu, X. Y.; Wang, A.; Lee, A. F.; Isaacs, M. A.; Li, L.; Pan, X.; Yang, X.; Wang, X.; Tai, Z.; et al. Ag Alloyed Pd Single-Atom Catalysts for Efficient Selective Hydrogenation of Acetylene to Ethylene in Excess Ethylene. *ACS Catal.* **2015**, *5*, 3717−3725.

(12) Lee, J. H.; Kim, S. K.; Ahn, I. Y.; Kim, W. J.; Moon, S. H. Performance of Pd−Ag/Al_2O_3 Catalysts Prepared by the Selective Deposition of Ag onto Pd in Acetylene Hydrogenation. *Catal. Commun.* **2011**, *12*, 1251−1254.

(13) Leviness, S.; Nair, V.; Weiss, A. H.; Schay, Z.; Guczi, L. Acetylene Hydrogenation Selectivity Control on PdCu/Al_2O_3 Catalysts. *J. Mol. Catal.* **1984**, *25*, 131−140.

(14) Guczi, L.; Schay, Z.; Stefler, G.; Liotta, L. F.; Deganello, G.; Venezia, A. M. Pumice-Supported Cu−Pd Catalysts: Influence of Copper on the Activity and Selectivity of Palladium in the Hydrogenation of Phenylacetylene and But-1-ene. *J. Catal.* **1999**, *182*, 456−462.

(15) Zhang, Q. W.; Li, J.; Liu, X. X.; Zhu, Q. M. Synergetic Effect of Pd and Ag Dispersed on Al_2O_3 in the Selective Hydrogenation of Acetylene. *Appl. Catal., A* **2000**, *197*, 221−228.

(16) Zhang, Y.; Diao, W.; Williams, C. T.; Monnier, J. R. Selective Hydrogenation of Acetylene in Excess Ethylene Using Ag- and Au−Pd/SiO_2 Bimetallic Catalysts Prepared by Electroless Deposition. *Appl. Catal., A* **2014**, *469*, 419−426.

(17) Pei, G. X.; Liu, X. Y.; Yang, X. F.; Zhang, L. L.; Wang, A. Q.; Li, L.; Wang, H.; Wang, X. D.; Zhang, T. Performance of Cu-Alloyed Pd Single-Atom Catalyst for Semihydrogenation of Acetylene under Simulated Front-End Conditions. *ACS Catal.* **2017**, *7*, 1491−1500.

(18) Wehrli, J. T.; Thomas, D. J.; Wainwright, M. S.; Trimm, D. L.; Cant, N. W. Selective Hydrogenation of Propyne over Supported Copper Catalysts: Influence of Support. *Appl. Catal.* **1991**, *70*, 253−262.

DOI: 10.1021/acs.jpcc.9b01757
J. Phys. Chem. C 2019, 123, 16107−16117

(19) Stammbach, M. R.; Thomas, D. J.; Trimm, D. L.; Wainwright, M. S. Hydrogenation of Ethyne over an Ion-Exchanged Copper on Silica Catalyst. *Appl. Catal.* **1990**, *58*, 209−217.
(20) McCue, A. J.; McRitchie, C. J.; Shepherd, A. M.; Anderson, J. A. Cu/Al_2O_3 Catalysts Modified with Pd for Selective Acetylene Hydrogenation. *J. Catal.* **2014**, *319*, 127−135.
(21) Bridier, B.; Hevia, M. A. G.; López, N.; Pérez-Ramírez, J. Permanent Alkene Selectivity Enhancement in Copper-Catalyzed Propyne Hydrogenation by Temporary CO Supply. *J. Catal.* **2011**, *278*, 167−172.
(22) Kyriakou, G.; Boucher, M. B.; Jewell, A. D.; Lewis, E. A.; Lawton, T. J.; Baber, A. E.; Tierney, H. L.; Stephanopoulos, M. F.; Sykes, E. C. H. Isolated Metal Atom Geometries as a Strategy for Selective Heterogeneous Hydrogenations. *Science* **2012**, *335*, 1209−1212.
(23) Fu, Q.; Luo, Y. Active Sites of Pd-Doped Flat and Stepped Cu(111) Surfaces for H_2 Dissociation in Heterogeneous Catalytic Hydrogenation. *ACS Catal.* **2013**, *3*, 1245−1252.
(24) Ghosh Chaudhuri, R.; Paria, S. Core/Shell Nanoparticles: Classes, Properties, Synthesis Mechanisms, Characterization, and Applications. *Chem. Rev.* **2012**, *112*, 2373−2433.
(25) Zhang, Q.; Lee, I.; Joo, J. B.; Zaera, F.; Yin, Y. Core−Shell Nanostructured Catalysts. *Acc. Chem. Res.* **2013**, *46*, 1816−1824.
(26) Feng, X.; Ling, L. X.; Cao, Y. T.; Zhang, R. G.; Fan, M. H.; Wang, B. J. A DFT Study on the Catalytic CO Oxidative Coupling to Dimethyl Oxalate on Al-Doped Core-Shell Pd Clusters. *J. Phys. Chem. C* **2018**, *122*, 1169−1179.
(27) Gao, H. L.; Liao, S. J.; Zeng, J. H.; Xie, Y. C.; Dang, D. Preparation and Characterization of Core−Shell Structured Catalysts Using Pt_xPd_y as Active Shell and Nano-Sized Ru as Core for Potential Direct Formic Acid Fuel Cell Application. *Electrochim. Acta* **2011**, *56*, 2024−2030.
(28) Li, S. J.; Cheng, D. J.; Qiu, X. G.; Cao, D. P. Synthesis of Cu@Pd Core-Shell Nanowires with Enhanced Activity and Stability for Formic Acid Oxidation. *Electrochim. Acta* **2014**, *143*, 44−48.
(29) Kuhn, M.; Lucas, M.; Claus, P. Long-Time Stability vs. Deactivation of $Pd-Ag/Al_2O_3$ Egg-Shell Catalysts in Selective Hydrogenation of Acetylene. *Ind. Eng. Chem. Res.* **2015**, *54*, 6683−6691.
(30) Guo, L.; Li, A. X.; An, X. Y.; Cao, Z. R.; Liu, N. Y. Catalytic Activity of $TM@Cu_{12}$ Core−Shell Nanoclusters for Water Gas Shift Reaction. *Int. J. Hydrogen Energy* **2015**, *40*, 8330−8340.
(31) Lin, J. H.; Guliants, V. V. Alumina-Supported Cu@Ni and Ni@Cu Core−Shell Nanoparticles: Synthesis, Characterization, and Catalytic Activity in Water−Gas-Shift Reaction. *Appl. Catal., A* **2012**, *445*−*446*, 187−194.
(32) McCue, A. J.; Baker, R. T.; Anderson, J. A. Acetylene Hydrogenation over Structured Au-Pd Catalysts. *Faraday Discuss.* **2016**, *188*, 499−523.
(33) Pérez-Carrillo, L. A.; Puca, M.; Rabelero, M.; Meza, K. E.; Puig, J. E.; Mendizábal, E.; López-Serrano, F.; López, R. G. Effect of Particle Size on the Mechanical Properties of Polystyrene and Poly(Butyl Acrylate) Core/Shell Polymers. *Polymer* **2007**, *48*, 1212−1218.
(34) Afremov, L.; Anisimov, S.; Iliushin, I. Size Effect on the Hysteresis Characteristics of a System of Interacting Core/Shell Nanoparticles. *J. Magn. Magn. Mater.* **2018**, *447*, 88−95.
(35) An, W.; Liu, P. Size and Shape Effects of Pd@Pt Core−Shell Nanoparticles: Unique Role of Surface Contraction and Local Structural Flexibility. *J. Phys. Chem. C* **2013**, *117*, 16144−16149.
(36) Gan, L.; Rudi, S.; Cui, C.; Heggen, M.; Strasser, P. Size-Controlled Synthesis of Sub-10 nm $PtNi_3$ Alloy Nanoparticles and their Unusual Volcano-Shaped Size Effect on ORR Electrocatalysis. *Small* **2016**, *12*, 3189−3196.
(37) Chen, H. M.; Xing, Z. L.; Zhu, S. Q.; Zhang, L. L.; Chang, Q. W.; Huang, J. L.; Cai, W. B.; Kang, N.; Zhong, C. J.; Shao, M. H. Palladium Modified Gold Nanoparticles as Electrocatalysts for Ethanol Electrooxidation. *J. Power Sources* **2016**, *321*, 264−269.
(38) Nørskov, J. K.; Bligaard, T.; Rossmeisl, J.; Christensen, C. H. Towards the Computational Design of Solid Catalysts. *Nat. Chem.* **2009**, *1*, 37−46.
(39) Delley, B. An All-Electron Numerical Method for Solving the Local Density Functional for Polyatomic Molecules. *J. Chem. Phys.* **1990**, *92*, 508−517.
(40) Tian, D. X.; Zhang, H. L.; Zhao, J. J. Structure and Structural Evolution of Ag_n(n = 3−22) Clusters Using a Genetic Algorithm and Density Functional Theory Method. *Solid State Commun.* **2007**, *144*, 174−179.
(41) Perdew, J. P.; Burke, K.; Ernzerhof, M. Generalized Gradient Approximation Made Simple. *Phys. Rev. Lett.* **1996**, *77*, 3865−3868.
(42) Dolg, M.; Wedig, U.; Stoll, H.; Preuss, H. Energy-Adjusted Ab initio Pseudopotentials for the First row Transition Elements. *J. Chem. Phys.* **1987**, *86*, 866−872.
(43) Inada, Y.; Orita, H. Efficiency of Numerical Basis Sets for Predicting the Binding Energies of Hydrogen Bonded Complexes: Evidence of Small Basis set Superposition Error Compared to Gaussian Basis Sets. *J. Comput. Chem.* **2008**, *29*, 225−232.
(44) Halgren, T. A.; Lipscomb, W. N. The Synchronous-Transit Method for Determining Reaction Pathways and Locating Molecular Transition States. *Chem. Phys. Lett.* **1977**, *49*, 225−232.
(45) Govind, N.; Petersen, M.; Fitzgerald, G.; King-Smith, D.; Andzelm, J. A Generalized Synchronous Transit Method for Transition State Location. *Comput. Mater. Sci.* **2003**, *28*, 250−258.
(46) Song, W.; Jiao, M. G.; Li, K.; Wang, Y.; Wu, Z. J. Theoretical Study on the Interaction of Pristine, Defective and Strained Graphene with Fe_n and Ni_n(n = 13, 38, 55) Clusters. *Chem. Phys. Lett.* **2013**, *588*, 203−207.
(47) Zhang, R. G.; Peng, M.; Duan, T.; Wang, B. J. Insight into Size Dependence of C_2 Oxygenate Synthesis from Syngas on Cu Cluster: The Effect of Cluster Size on the Selectivity. *Appl. Surf. Sci.* **2017**, *407*, 282−296.
(48) Zhang, R. G.; Zhao, B.; Ling, L. X.; Wang, A. J.; Russell, C. K.; Wang, B. J.; Fan, M. H. Cost-Effective Palladium-Doped Cu Bimetallic Materials to Tune Selectivity and Activity by using Doped Atom Ensembles as Active Sites for Efficient Removal of Acetylene from Ethylene. *ChemCatChem* **2018**, *10*, 2424−2432.
(49) Teschner, D.; Borsodi, J.; Wootsch, A.; Révay, Z.; Hävecker, M.; Knop-Gericke, A.; Jackson, S. D.; Schlögl, R. The Roles of Subsurface Carbon and Hydrogen in Palladium-Catalyzed Alkyne Hydrogenation. *Science* **2008**, *320*, 86−89.
(50) Studt, F.; Abild-Pedersen, F.; Bligaard, T.; Sørensen, R. Z.; Christensen, C. H.; Nørskov, J. K. On the Role of Surface Modifications of Palladium Catalysts in the Selective Hydrogenation of Acetylene. *Angew. Chem., Int. Ed.* **2008**, *47*, 9299−9302.
(51) García-Mota, M.; Bridier, B.; Pérez-Ramírez, J.; López, N. Interplay Between Carbon Monoxide, Hydrides, and Carbides in Selective Alkyne Hydrogenation on Palladium. *J. Catal.* **2010**, *273*, 92−102.
(52) Yang, B.; Burch, R.; Hardacre, C.; Headdock, G.; Hu, P. Influence of Surface Structures, Subsurface Carbon and Hydrogen, and Surface Alloying on the Activity and Selectivity of Acetylene Hydrogenation on Pd Surfaces: A Density Functional Theory Study. *J. Catal.* **2013**, *305*, 264−276.
(53) Galipaud, J.; Martin, M. H.; Roué, L.; Guay, D. Measurement of Hydrogen Solubility in Pd_xCu_{100-x} Thin Films Prepared by Pulsed Laser Deposition: An Electrochemical in Situ X-Ray Diffraction Analysis. *J. Phys. Chem. C* **2013**, *117*, 2688−2698.
(54) Yang, B.; Burch, R.; Hardacre, C.; Headdock, G.; Hu, P. Origin of the Increase of Activity and Selectivity of Nickel Doped by Au, Ag, and Cu for Acetylene Hydrogenation. *ACS Catal.* **2012**, *2*, 1027−1032.
(55) Sheth, P. A.; Neurock, M.; Smith, C. M. A First-Principles Analysis of Acetylene Hydrogenation over Pd(111). *J. Phys. Chem. B* **2003**, *107*, 2009−2017.
(56) Yang, J.; Cao, L. X.; Wang, G. C. Acetylene Hydrogenation on Anatase TiO_2(101) Supported Pd_4 Cluster: Oxygen Deficiency Effect. *J. Mol. Model.* **2012**, *18*, 3329−3339.

DOI: 10.1021/acs.jpcc.9b01757
J. Phys. Chem. C 2019, 123, 16107−16117

(57) Meng, L. D.; Wang, G. C. A DFT + U Study of Acetylene Selective Hydrogenation over Anatase Supported Pd_aAg_b (a + b = 4) Cluster. *Phys. Chem. Chem. Phys.* **2014**, *16*, 17541−17550.
(58) Xu, L.; Stangland, E. E.; Mavrikakis, M. Ethylene versus ethane: A DFT-based selectivity descriptor for efficient catalyst screening. *J. Catal.* **2018**, *362*, 18−24.
(59) Cao, X. M.; Burch, R.; Hardacre, C.; Hu, P. An Understanding of Chemoselective Hydrogenation on Crotonaldehyde over Pt(111) in the Free Energy Landscape: The Microkinetics Study Based on First Principles Calculations. *Catal. Today* **2011**, *165*, 71−79.
(60) Zhang, R. G.; Zhang, J.; Zhao, B.; He, L. L.; Wang, A. J.; Wang, B. J. Insight into the Effects of Cu Component and the Promoter on the Selectivity and Activity for Efficient Removal of Acetylene from Ethylene on Cu-Based Catalyst. *J. Phys. Chem. C* **2017**, *121*, 27936−27949.
(61) Cheng, J.; Hu, P. Theory of the Kinetics of Chemical Potentials in Heterogeneous Catalysis. *Angew. Chem., Int. Ed.* **2011**, *50*, 7650−7654.
(62) Cheng, J.; Hu, P.; Ellis, P.; French, S.; Kelly, G.; Lok, C. M. Brønsted-Evans-Polanyi Relation of Multistep Reactions and Volcano Curve in Heterogeneous Catalysis. *J. Phys. Chem. C* **2008**, *112*, 1308−1311.
(63) Pallassana, V.; Neurock, M. Electronic Factors Governing Ethylene Hydrogenation and Dehydrogenation Activity of Pseudomorphic Pd_{ml}/Re(0001), Pd_{ml}/Ru(0001), Pd(111), and Pd_{ml}/Au(111) Surfaces. *J. Catal.* **2000**, *191*, 301−317.
(64) Zhang, R. G.; Zhao, B.; He, L. L.; Wang, A. J.; Wang, B. J. Cost-Effective Promoter-Doped Cu-Based Bimetallic Catalysts for the Selective Hydrogenation of C_2H_2 to C_2H_4: the Effect of the Promoter on Selectivity and Activity. *Phys. Chem. Chem. Phys.* **2018**, *20*, 17487−17496.
(65) Zhao, B.; Zhang, R. G.; Huang, Z. X.; Wang, B. J. Effect of the Size of Cu Clusters on Selectivity and Activity of Acetylene Selective Hydrogenation. *Appl. Catal., A* **2017**, *546*, 111−121.

DOI: 10.1021/acs.jpcc.9b01757
J. Phys. Chem. C 2019, 123, 16107−16117